Proceedings of the ASME 2025
International Design Engineering Technical Conferences and
Computers and Information in Engineering Conference
IDETC/CIE2025
August 17–20, 2025, Anaheim, California

IDETC/CIE2024: 168733

CONSTRAINED BAYESIAN OPTIMIZATION FOR ROBUST DESIGN OF COMPLEX SYSTEMS UNDER VARYING OPERATING CONDITIONS

Siyu Chen, Stephen Bierschenk, Desiderio Kovar, Zhenghui Sha*,

Walker Department of Mechanical Engineering, The University of Texas at Austin, Austin, TX

ABSTRACT

Engineering design optimization of complex systems often involves varying operating conditions, e.g., the same design of a cold-spray nozzle under different manufacturing configurations with varying pressures and stand-off distance. This requires robust design methods to simultaneously ensure high performance and the stability of such a high performance. This paper presents a constrained Bayesian Optimization (BO) framework for robust design, aimed at optimizing performance and stability across varying operation conditions or configurations. The proposed methodology leverages condition-specific Gaussian Process (GP) submodels to estimate the nonlinear relationships between design parameters and performance using a newly developed robust Expected Improvement (EI) acquisition function. This function aggregates GP submodels from different configurations accounting for the worst-case scenario, a strategy that selects the minimum posterior mean and maximum posterior variance across the submodels to prioritize the most challenging scenario from all operating conditions. In addition, a penalty term based on the variance of the posterior mean is added to the new EI acquisition function to improve the consistency of the design performance. To demonstrate its effectiveness, we applied the framework to the design optimization of cold spray nozzles, where the objective is to find dimension variables of the nozzle that maximize particle impact velocity while ensuring a stable performance under four operating conditions. The results demonstrate that the proposed approach achieves high performance, with a 13% improvement over the original design. Furthermore, the performance variance is reduced from 204.97 $(m/s)^2$ to 43.06 $(m/s)^2$, significantly improving the design consistency. These results highlight its potential for broader applications in robust engineering design optimization.

Keywords: Bayesian Optimization, Robust Design, Design Space Exploration

*Corresponding author: zsha@austin.utexas.edu
Documentation for `asmeconf.cls`: Version 1.40, May 17, 2025.

1. INTRODUCTION

Engineering design optimization often involves complex systems characterized by black-box objective functions, nonlinear relationships, and intricate interactions among design parameters. In these scenarios, the explicit mathematical relationship between input parameters and desired performance metrics is typically unknown or computationally expensive to evaluate directly [1]. This complexity poses significant challenges for traditional optimization methods, motivating the development of data-driven, surrogate-based optimization approaches that efficiently explore high-dimensional design spaces [2].

Bayesian Optimization (BO) has emerged as a powerful data-driven solution to these challenges by effectively balancing exploration and exploitation in engineering design optimization [3]. BO utilizes probabilistic surrogate models, typically Gaussian Processes (GP), to approximate unknown objective functions while quantifying uncertainty in predictions [4]. This uncertainty estimation enables BO to strategically balance exploration and exploitation, efficiently identifying promising regions and reducing computational costs, particularly for expensive evaluations such as high-dimensional simulations or physical experiments.

However, applying BO to engineering design introduces many practical challenges. Engineering systems frequently operate under varying conditions or constraints, making them challenging to achieve high performance [5]. However, robustness is critical, as designs must not only perform well under nominal conditions, but also remain stable under varied operational scenarios. For instance, in our study on nozzle geometry optimization, performance metrics such as particle impact velocity must be maximized and maintained consistently despite variations in operating parameters [6]. Similarly, such a challenge arises in many other engineering domains, including aerodynamic shape optimization, where airfoil designs must deliver consistent lift and drag characteristics under different flow conditions [7]; structural optimization, where designs must reliably withstand varying load cases and uncertainties in material properties [8]; and thermal

management systems, where optimal cooling performance must be preserved across fluctuating operating temperatures [9].

Recent advancements in BO have introduced both constrained BO and robust BO methods to address performance uncertainties and feasibility constraints in complex engineering designs. Constrained BO aims to optimize the objective functions while ensuring feasibility under predefined constraints. To improve optimization efficiency, recent studies have integrated constraint-awareness into surrogate models [10], developed merit-based trade-offs to balance objective improvement with constraint satisfaction [11], and incorporated predictive strategies to anticipate and manage future feasibility challenges [12]. These advances collectively improved the reliability and practicality of constrained BO.

On the other hand, robust BO methods aim to improve performance consistency across uncertain conditions. In particular, approaches such as Robust Expected Improvement (REI) incorporate adversarial strategies to enhance robustness [13–15]. However, existing robust BO methods emphasize worst-case performance optimization without explicitly balancing performance maximization and robustness across varying conditions.

Despite these advancements, a critical gap remains in integrating both constraint handling and robustness within a unified BO framework. Although constrained BO ensures feasibility, it does not explicitly address robustness, which is crucial for engineering applications where designs must perform consistently under variable conditions. In contrast, robust BO focuses on worst-case performance, but does not guarantee constraint satisfaction. Bridging this gap requires developing a joint constrained and robust BO framework that ensures both high performance and stability in uncertain and constrained design spaces.

This paper is motivated to address this gap, thereby presenting a constrained Bayesian Optimization (BO) framework for robust design. The proposed methodology employs condition-specific Gaussian Process (GP) submodels to model the nonlinear relationships between design parameters and performance under different configurations. To ensure robustness, we develop a novel Expected Improvement (EI) acquisition function that aggregates GP submodels by prioritizing the worst-case scenario—selecting the minimum posterior mean and maximum posterior variance across conditions. Additionally, a penalty term based on the variance of the posterior means is incorporated into the EI function to enhance consistency, preventing designs that are highly sensitive to operating variations. This approach effectively balances exploration and exploitation, guiding the search toward high-performance and stable designs. To validate its effectiveness, we applied the framework to the design optimization of cold spray nozzles, where the goal is to maximize particle impact velocity while ensuring stable performance across four operating conditions. The results demonstrate a 13% improvement in impact velocity over the original design. Additionally, the performance variance is significantly reduced from 204.97 $(m/s)^2$ to 43.06 $(m/s)^2$, enhancing design consistency. These findings highlight the broader applicability of the proposed approach for robust engineering design optimization.

The remainder of this paper is structured as follows. Section 2 provides the technical background, including an overview of constrained optimization problems and the GP surrogate model, along with the role of acquisition functions. Section 3 introduces the proposed constrained BO framework for robust design. This section details the constraint GP modeling approach and the robust EI acquisition function that optimizes the design performance under uncertainties and its consistency. Section 4 demonstrates this framework in a cold-spray nozzle design problem. This section presents the experimental setup and results, including convergence behavior and validation of the GP regression model. Finally, Section 5 summarizes our key findings, potential limitations, and future research directions.

2. TECHNICAL BACKGROUND

2.1. Constrained Optimization Problem

The constrained optimization problem aims to maximize an objective function $f(\mathbf{x}) : \mathbb{R}^n \to \mathbb{R}$, where $\mathbf{x} \in \mathbb{R}^n$ denotes the vector of design variables, subject to both equality and inequality constraints. This formulation is expressed as:

$$\max_{\mathbf{x}} f(\mathbf{x}) \tag{1}$$

$$\max_{\mathbf{x}} f(\mathbf{x}) \tag{2}$$

subject to:

$$g_i(\mathbf{x}) \leq 0, \quad i = 1, 2, \ldots, p \tag{3}$$

$$h_j(\mathbf{x}) = 0, \quad j = 1, 2, \ldots, m. \tag{4}$$

Here, $f(\mathbf{x})$ evaluates the performance or quality of the design $\mathbf{x}$, while $g_i(\mathbf{x})$ and $h_j(\mathbf{x})$ represent the inequality and equality constraint functions, respectively. The feasible region is defined by the set of solutions that satisfy all constraints. The goal of the optimization is to identify an optimal solution $\mathbf{x}^*$ such that:

$$f(\mathbf{x}^*) \geq f(\mathbf{x}), \quad \forall \mathbf{x} \text{ satisfying (3) and (4).} \tag{5}$$

We note that this study focuses exclusively on equality constraints, as the design configurations under consideration are most appropriately and conventionally formulated using equality conditions.

2.2. Bayesian Optimization

BO is a sequential optimization strategy that efficiently explores high-dimensional design spaces to optimize unknown objective functions. BO leverages a probabilistic surrogate model, such as GP, and an acquisition function (AF) to guide the selection of the next sampling point.

2.2.1. Gaussian Process Surrogate Model GP regression provides a flexible and probabilistic model for approximating the objective function $f(\mathbf{x})$ based on observed data $\mathcal{D} = \{(\mathbf{x}_i, y_i)\}_{i=1}^k$. A GP is defined by its mean function, typically assumed to be zero, and a covariance function (kernel) that encodes prior assumptions about smoothness and correlation [16]:

$$f(\mathbf{x}) \sim \mathcal{GP}(\mu(\mathbf{x}), \Sigma(\mathbf{x}, \mathbf{x}')), \tag{6}$$

where $\mu(\mathbf{x})$ is the mean function and $\Sigma(\mathbf{x}, \mathbf{x}')$ is the covariance function that determines the correlation between function values at different input locations.

In this study, a rational quadratic kernel (see Eq. (7)) was adopted due to its ability to model functions with varying smoothness across the design space [17]. Unlike the widely used squared exponential (SE) kernel, which assumes a single lengthscale l for the entire input space, the rational quadratic kernel introduces a power parameter α that enables it to capture both short-range and long-range dependencies in the objective function. This makes it particularly well-suited for optimization tasks where different regions of the design space exhibit varying sensitivity to input parameters.

$$\Sigma(\mathbf{x}, \mathbf{x}') = \sigma^2 \left(1 + \frac{\|\mathbf{x} - \mathbf{x}'\|^2}{2\alpha l^2}\right)^{-\alpha}, \tag{7}$$

where σ^2 controls the output variance, l represents the characteristic lengthscale, and α determines the relative weighting of short- and long-range correlations. The choice of this kernel allows the model to adapt to potential local irregularities while maintaining overall smoothness, improving the exploration-exploitation balance in the optimization process.

After observing data, the posterior distribution of $f(\mathbf{x})$ is also Gaussian:

$$f(\mathbf{x}) \mid \mathcal{D} \sim \mathcal{GP}(\mu_{\text{post}}(\mathbf{x}), \sigma^2_{\text{post}}(\mathbf{x})),$$

with:

$$\mu_{\text{post}}(\mathbf{x}) = \mathbf{\Sigma}(\mathbf{x}, \mathbf{x}_{1:k})\mathbf{\Sigma}^{-1}(\mathbf{x}_{1:k}, \mathbf{x}_{1:k})\mathbf{y}, \tag{8}$$

$$\sigma^2_{\text{post}}(\mathbf{x}) = \Sigma(\mathbf{x}, \mathbf{x}) - \mathbf{\Sigma}(\mathbf{x}, \mathbf{x}_{1:k})\mathbf{\Sigma}^{-1}(\mathbf{x}_{1:k}, \mathbf{x}_{1:k})\mathbf{\Sigma}(\mathbf{x}_{1:k}, \mathbf{x}), \tag{9}$$

where $\mathbf{\Sigma}$ represents the covariance matrix of the observations. The posterior mean $\mu_{\text{post}}(\mathbf{x})$ provides the predicted function value, and the variance $\sigma^2_{\text{post}}(\mathbf{x})$ quantifies the uncertainty.

2.2.2. Acquisition Function AF is a key component of BO, responsible for determining the next sampling point within the design space. It leverages the probabilistic surrogate model, described in Section 2.2.1, to approximate the objective function and guide the optimization process. At each iteration, AF is optimized to identify the most promising candidate for evaluation [3]. The primary role of AF is to balance the trade-off between exploration, which seeks to improve the model by sampling uncertain regions, and exploitation, which prioritizes regions with known high-performance solutions.

Among the various available AFs, the expected improvement (EI) [5] (see Eq. (10)) is widely used due to its ability to effectively balance this trade-off. Unlike purely exploitation-based approaches, EI accounts for both the predicted improvement over the current best solution and the uncertainty of predictions, making it particularly useful when the objective function is expensive to evaluate. By selecting points that have both high predicted improvement and high uncertainty, EI ensures a well-balanced search strategy, leading to more efficient convergence in design optimization tasks.

$$a_{\text{EI}}(\mathbf{x}) = \left(\mu_{\text{post}}(\mathbf{x}) - f_{\text{best}} - \xi\right)\Phi(z) + \sigma_{\text{post}}(\mathbf{x})\phi(z), \tag{10}$$

where:

$$z = \frac{\mu_{\text{post}}(\mathbf{x}) - f_{\text{best}} - \xi}{\sigma_{\text{post}}(\mathbf{x})}.$$

Here, $\mu_{\text{post}}(\mathbf{x})$ and $\sigma_{\text{post}}(\mathbf{x})$ are the posterior mean and standard deviation of the GP model, respectively. $\Phi(z)$ and $\phi(z)$ are the cumulative distribution function (CDF) and probability density function (PDF) of the standard normal distribution, f_{best} represents the best observed function value so far, and ξ is an exploration parameter that controls the balance between exploration and exploitation. The next sampling point, $\mathbf{x}^*$, is determined by maximizing the acquisition function:

$$\mathbf{x}^* = \arg\max a_{\text{EI}}(\mathbf{x}). \tag{11}$$

3. CONSTRAINED BAYESIAN OPTIMIZATION FOR ROBUST DESIGN

The proposed Constrained Bayesian Optimization for Robust Design is a probabilistic framework that optimizes an objective function while satisfying constraints and ensuring robust performance across varying conditions. This study aims to develop an efficient BO approach that not only maximizes design performance but also enhances its consistency across multiple conditions (constraints). Therefore, the proposed framework is divided into two key steps: constraint GP modeling and robust EI optimization, as illustrated in Figure 1 and detailed in the following subsections.

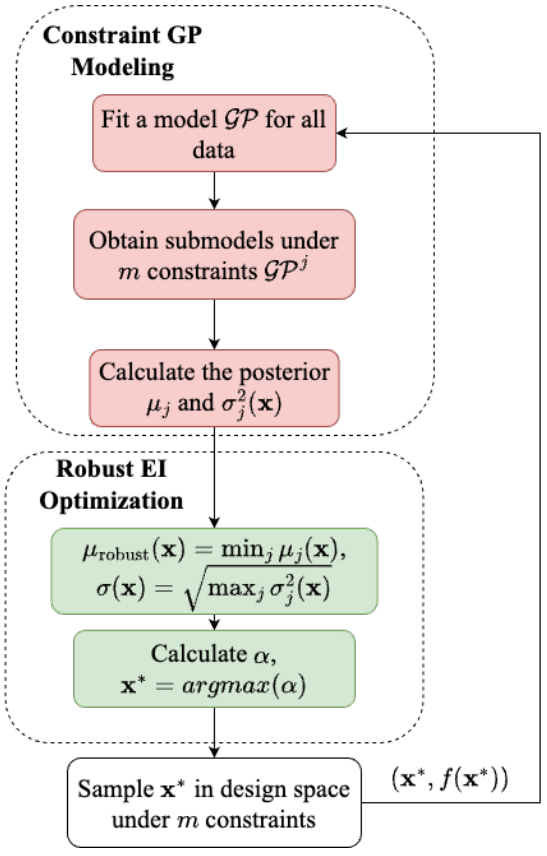

FIGURE 1: FLOWCHART OF THE CONSTRAINED BAYESIAN OPTIMIZATION FRAMEWORK FOR ROBUST DESIGN.

3.1. Constraint Gaussian Process (GP) Modeling

The process begins by fitting a GP model ($\mathcal{GP}$) to the entire dataset. This model captures complex, nonlinear relationships between design variables and the objective function, providing the predicted mean ($\mu(\mathbf{x})$) and variance ($\sigma^2(\mathbf{x})$) as a surrogate for the true function. To account for constraints, the GP model is evaluated under m specific constrained conditions, resulting in condition-specific GP submodels ($\mathcal{GP}^j$) for $j = 1, 2, \ldots, m$. For each submodel, the GP predicts the mean ($\mu^j(\mathbf{x})$) and variance ($\sigma^{2j}(\mathbf{x})$) of the objective function.

3.2. Robust Expected Improvement (EI) Optimization

In this study, we develop a robust EI function to balance the trade-off between two objectives, maximizing performance and ensuring its consistency across different conditions.

3.2.1. Performance First, to maximize *performance* across varying conditions, the robust EI approach incorporates a mechanism that accounts for the expected worst-case performance. By extending Eq. (10), this formulation ensures that the selected designs achieve high performance under fluctuating operating parameters. The robust EI is defined as:

$$EI(\mathbf{x}) = (\mu_{\text{robust}}(\mathbf{x}) - f_{\text{best}} - \xi)\Phi(z) + \sigma(\mathbf{x})\phi(z), \tag{12}$$

where:

- $\mu_{\text{robust}}(\mathbf{x}) = \min_j \mu_j(\mathbf{x})$ represents the worst-case expected impact velocity across all conditions. By prioritizing the lowest predicted performance, this term ensures that the selected design maintains high performance even in the least favorable scenario, thereby enhancing robustness.
- $\sigma(\mathbf{x}) = \sqrt{\max_j \sigma_j^2(\mathbf{x})}$ avoids high-variance regions that could lead to unstable performance.
- f_{best} is the highest average performance observed under varying conditions, defined as:

$$f_{\text{best}} = \max_{k \in \mathcal{K}} \frac{1}{m} \sum_{j=1}^{m} f_j(\mathbf{x}_k), \tag{13}$$

  where $\mathcal{K}$ represents the set of designs evaluated previously and m is the number of operating conditions.
- The standardized variable z is defined as:

$$z = \frac{\mu_{\text{robust}}(\mathbf{x}) - f_{\text{best}} - \xi}{\sigma(\mathbf{x})}, \tag{14}$$

  which measures the expected improvement over the current best solution, normalized by the predictive uncertainty. The parameter $\xi \geq 0$ is a user-defined exploration parameter that controls the trade-off between exploitation and exploration. A smaller z increases the influence of the uncertainty term, promoting exploration in regions where the model is less confident.

By defining $\mu_{\text{robust}}(\mathbf{x})$ as the minimum posterior mean across conditions, we prioritize the worst-case expected performance, ensuring robustness against fluctuating operating conditions. Similarly, using $\sigma(\mathbf{x}) = \sqrt{\max_j \sigma_j^2(\mathbf{x})}$ captures the highest uncertainty, preventing selection of unstable designs. The combination of these two operations leads to a decreased value of the standardized z-score z in Euqation (14), reducing $\Phi(z)$ and increasing $\phi(z)$, thereby naturally shifting the acquisition function toward exploration. As a result, the proposed robust EI formulation not only enhances performance under the worst-case scenario, but also promotes exploration, improving optimization efficiency in uncertain design spaces. It is important to note that this formulation assumes that the posterior mean, variance, and best observed performance f_{best} are treated under a consistent Gaussian assumption, despite being derived from different submodels.

3.2.2. Consistency Second, to ensure *consistency* across different operating conditions, we introduce a penalty term that quantifies the variability of the expected impact velocity:

$$\text{P}(\mathbf{x}) = \text{Var}(\mu_j(\mathbf{x})), \tag{15}$$

where $\mu_j(\mathbf{x})$ represents the expected performance for each condition j. A higher penalty value indicates greater variability across conditions, which is less favorable, discouraging solutions with inconsistent performance.

To ensure comparability between the EI values and the variance penalty in the acquisition function, both terms are normalized using min-max scaling:

$$\text{Normalized EI}(\mathbf{x}) = \frac{EI(\mathbf{x}) - \min(EI)}{\max(EI) - \min(EI)} \tag{16}$$

$$\text{Normalized P}(\mathbf{x}) = \frac{\text{P}(\mathbf{x}) - \min(\text{P})}{\max(\text{P}) - \min(\text{P})} \tag{17}$$

This ensures that both terms are within the same numerical range $[0, 1]$, making them directly comparable when applying the penalty weight. The final EI function is formulated as:

$$\alpha(\mathbf{x}) = \text{Normalized EI}(\mathbf{x}) - \lambda \cdot \text{Normalized P}(\mathbf{x}), \tag{18}$$

where λ is a user-defined parameter that controls the trade-off between maximizing performance and ensuring robustness across conditions. A higher λ value places greater emphasis on minimizing variability, favoring solutions with stable performance across conditions. Conversely, a lower λ prioritizes higher performance while allowing greater variability.

The next sampling point $\mathbf{x}^*$ is determined by maximizing the robust EI:

$$\mathbf{x}^* = \arg\max \alpha(\mathbf{x}). \tag{19}$$

The selected point is evaluated under all constrained conditions and the new observations $(\mathbf{x}^*, f(\mathbf{x}^*))$ are incorporated into the training dataset. The GP model is re-trained and the iterative process is repeated until convergence or a predefined number of iterations is reached.

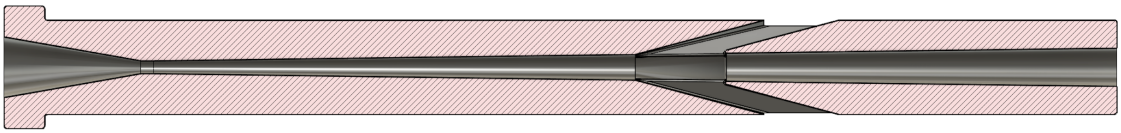

(a) Nozzle cross-section.

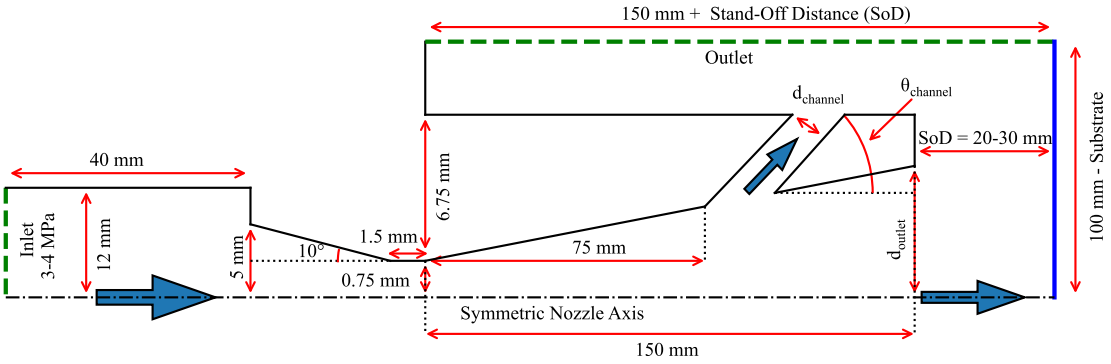

(b) Geometric parameters for optimization.

FIGURE 2: NOZZLE GEOMETRY [18]. THE OBJECTIVE IS TO MAXIMIZE PARTICLE IMPACT VELOCITY BY OPTIMIZING GEOMETRIC PARAMETERS, INCLUDING THE CHANNEL ANGLE (θ_{channel}), CHANNEL DIAMETER (d_{channel}), AND OUTLET DIAMETER (d_{outlet}), UNDER VARYING OPERATIONAL CONDITIONS DEFINED BY INLET PRESSURE (IP) AND STAND-OFF DISTANCE (SoD).

4. CASE STUDY: NOZZLE DESIGN FOR COLD SPRAY

4.1. Background of Cold Spray

The optimization of cold spray nozzles is essential for particle impact velocity, a critical factor influencing both film quality and deposition efficiency. Conventional nozzle designs often suffer from stagnation pressure build-up downstream of the bow shock, which can significantly reduce the velocities of fine particles, below 10 μm, as they travel through the stagnant gas [19, 20]. Recent studies of the micro-cold spray process, a lower pressure spray process, have shown that the introduction of pressure relief channels into the nozzle diverging region can significantly reduce particle slowing across the bow shock [6, 18]. In this case study, we employ constrained Bayesian optimization to find the best design of pressure relief channel features, as described in Section 3, to enhance the fine particle velocities and the performance consistency under different operating conditions.

As illustrated in Figure 2, the optimization process focuses on three key geometric parameters: the channel angle (θ_{channel}), channel diameter (d_{channel}), and outlet diameter (d_{outlet}). The channel angle governs the direction of the flow exiting the nozzle diverging region, and the channel diameter determines the volume of the flow exiting the nozzle diverging region. The outlet diameter controls the nozzle expansion ratio (i.e. the rate of gas expansion in the nozzle). These parameters affect the amount of gas allowed to escape the nozzle diverging region, the velocity and dispersion characteristics of the particles within the nozzle, and the location of the bow shock and other shock waves that occur around the channels themselves.

In addition to these geometric parameters, the design incorporates operational constraints, such as inlet pressure and stand-off distance. The inlet pressure provides the initial energy required to accelerate particles, while the stand-off distance, defined as the gap between the nozzle and the substrate, directly affects the location and pressure difference across the bow shock. Parameters were selected to include a range of commonly used pressures and stand-off distances used in high-pressure cold spray. Large variations in fine particle velocity are observed depending on the choice of inlet pressure and stand-off distance. By optimizing particle velocities over a range of operating conditions, the resulting nozzle geometry will be relevant to a wide range of materials specific spraying conditions. Other system parameters such as gas type (nitrogen), outlet pressure (1 atm), particle diameter ($1\mu m$, and particle material (alumina, density=$3.95 g/cm^3$) were held constant.

By systematically optimizing these geometric and operational parameters, the proposed nozzle design achieved higher impact velocities for fine particles, leading to improved deposition efficiency and allowing for the deposition of brittle materials such as ceramics which require fine particle sizes for deposition via cold spray [21].

4.2. Problem Formulation

The objective of this case study is to maximize the particle impact velocity (V) while ensuring its consistency under varying operational conditions. Fine particles, significantly influenced by the bow shock, are optimized by adjusting the geometric parameters: channel angle (x_1), channel diameter (x_2) and outlet diameter (x_3). The impact velocity is modeled as a function of these three geometric parameters along with two operational

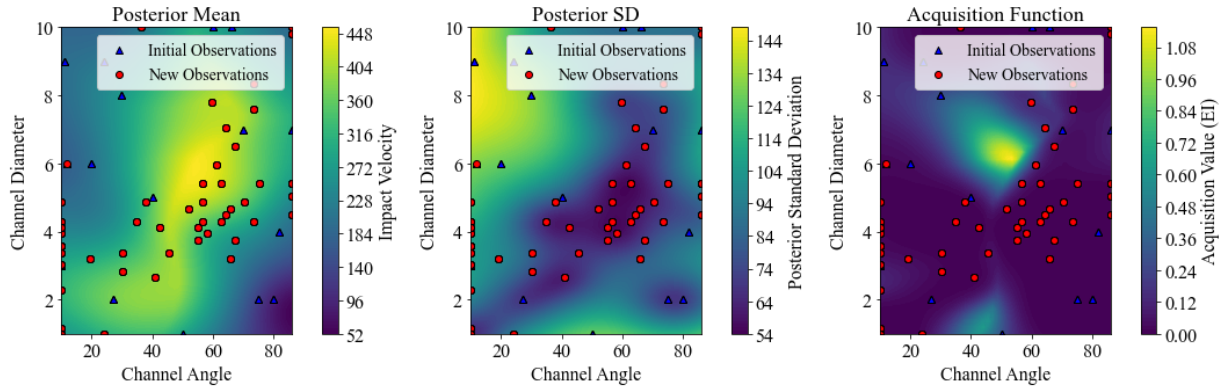

FIGURE 3: POSTERIOR MEAN, STANDARD DEVIATION, AND ACQUISITION FUNCTION FOR THE DESIGN SPACE. THE OVERLAID POINTS REPRESENT ALL SIMULATION OBSERVATIONS, WITH BLUE TRIANGLES INDICATING THE INITIAL 64 OBSERVATIONS AND RED DOTS SHOWING THE 212 ADDITIONAL POINTS SELECTED BY THE PROPOSED APPROACH.

parameters, inlet pressure (IP) and stand-off distance (SoD):

$$V = f(x_1, x_2, x_3, IP, SoD). \tag{20}$$

The constrained Bayesian optimization framework for robust design is applied to solve this problem, where the geometric parameters ($\mathbf{x} = [x_1, x_2, x_3]$) serve as decision variables, and the operating parameters (IP and SoD) define the constraints. The four constraints ($m = 4$) correspond to specific operational scenarios, with each scenario fixing IP and SoD as follows:

$$\begin{aligned} h_1(\mathbf{x}): &\quad IP = 3\,MPa,\ SoD = 20\,mm, \\ h_2(\mathbf{x}): &\quad IP = 3\,MPa,\ SoD = 30\,mm, \\ h_3(\mathbf{x}): &\quad IP = 4\,MPa,\ SoD = 20\,mm, \\ h_4(\mathbf{x}): &\quad IP = 4\,MPa,\ SoD = 30\,mm. \end{aligned} \tag{21}$$

For each scenario $j \in \{1, 2, 3, 4\}$, the particle impact velocity is represented as $f_j(x_1, x_2, x_3)$, with IP and SoD fixed to the corresponding values. To ensure both high performance and consistency across all operational scenarios, the optimization problem is formulated with two key objectives:

- **Maximizing performance:** The optimization aims to maximize robust expected improvement, ensuring both high impact velocity and balanced exploration under varying conditions. As defined in Section 3.2, the EI formulation follows Eq. (12).

- **Ensuring consistency:** To penalize high variability in performance across different operating conditions, we incorporate the consistency term $\mathrm{P}(\mathbf{x})$, as defined in Eq. (15). This term discourages solutions with large deviations in expected impact velocity across conditions.

By normalizing and integrating both objectives, the final optimization problem is formulated as Eq. (19) to ensures high impact velocity while maintaining consistency across varying conditions, as constrained in Eq. (21).

4.3. Experimental Settings

In the BO framework, a GP surrogate model was employed to capture the nonlinear relationship between the impact velocity (V) and geometric parameters and operating parameters. The GP model utilized a rational quadratic kernel, defined in Eq. (7), with a lengthscale of $l = 1.0$, power $\alpha = 1.5$, and variance $\sigma^2 = 1.0$.

The optimization began with an initial dataset comprising 64 points (16 sets), sampled from the design space. The design parameter ranges were defined as follows: channel angle (x_1) from 10° to 86°, channel diameter (x_2) from 1 mm to 10 mm, and outlet diameter (x_3) from 3 mm to 13 mm. A robust EI acquisition function, formulated in Eq. (18), guided the selection of new samples at each iteration, with an exploration parameter of $\xi = 1.0$ to effectively balance exploration and exploitation. In addition, λ is set as 1 for each iteration to balance the trade-off between high performance and small variation. The optimization process continued over 53 iterations, adding four new samples (one set) per iteration, resulting in a total of 276 points (69 sets) evaluated to refine the design space and maximize V.

A steady-state solution to the gas flow profile within the nozzle were calculated using the COMSOL Multiphysics Computational Fluid Dynamics Module [22]. Particle velocities along the nozzle axis were calculated using the drag model developed by Henderson [23].

4.4. Experimental Results

4.4.1. Convergence for optimal nozzle design Figure 4 illustrates the convergence of the best observed average impact velocity across iterations. The x-axis represents the iteration number, and the y-axis shows the observed average impact velocity. Table 1 further compares the initial and optimal nozzle designs in terms of both performance and consistency. The optimal design achieves a higher impact velocity of 538 m/s compared to 477 m/s in the initial design, reflecting a significant performance improvement. Additionally, the consistency, measured by the variance of impact velocity across operating conditions, improves from 204.93 $(m/s)^2$ in the initial design to 43.06 $(m/s)^2$ in the optimal design, demonstrating enhanced robustness.

TABLE 1: THE COMPARISON BETWEEN INITIAL DESIGN AND OPTIMAL DESIGN.

	Initial Design	Optimal Design
Design Parameters [channel angle, channel dia., outlet dia.]	[10.00°, 3.00 mm, 10.00 mm]	[53.43°, 6.14 mm, 5.65 mm]
Performance (impact velocity)	478.25 m/s	538.25 m/s
Consistency (variance)	204.93 $(m/s)^2$	43.06 $(m/s)^2$

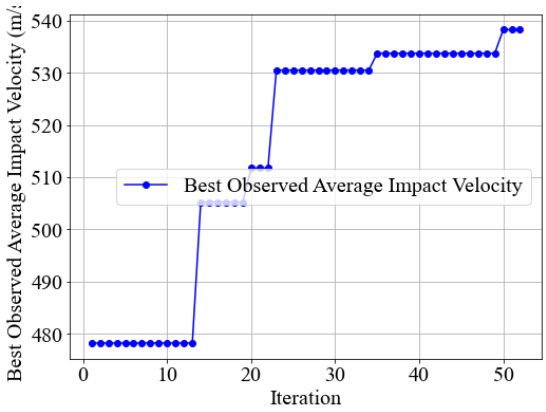

FIGURE 4: CONVERGENCE FOR FINDING THE AVERAGE IMPACT VELOCITY ACROSS FOUR CONDITIONS.

Figure 3 illustrates the surrogate model $\mathcal{GP}$ for the design space in Eq. (20), where blue triangles represent the initial dataset (64 points), and red dots denote the additional 212 points selected by the proposed approach. The plots display the posterior mean, posterior standard deviation (SD), and acquisition function (EI) derived from a three-dimensional design space. To show robustness of the performance, the impact velocity (V) is averaged across four operational conditions. For better visualization, the outlet diameter is fixed at 5.65 mm, reducing the design space to two dimensions: channel angle and channel diameter. The following description provides a detailed analysis of the GP posterior mean, standard deviation, and acquisition function.

- **Posterior Mean (Leftmost Plot of Figure 3):** The posterior mean highlights regions with high predicted impact velocity (V), represented by brighter colors (yellow). The best design candidates are concentrated in the region with a *channel angle of approximately 50–70 degrees* and a *channel diameter of 5–8 mm*, where the predicted impact velocity is maximized. These regions indicate the surrogate model's ability to identify promising design configurations, demonstrating an optimal balance between input parameters for achieving high-performance outcomes.
- **Posterior Standard Deviation (Middle Plot of Figure 3):** The posterior SD visualizes the uncertainty of the GP model's predictions, where brighter colors indicate higher uncertainty. The highest uncertainty is observed in sparsely sampled regions, particularly near the *upper left and lower right corners of the design space*, as well as in areas with limited observations, such as around a *channel angle below 30 degrees and a channel diameter above 8 mm*. This suggests that additional sampling in these regions could improve model confidence and prediction accuracy. The uncertainty pattern aligns with Bayesian optimization principles, emphasizing increased variance in unexplored regions.
- **Acquisition Function (Rightmost Plot of Figure 3):** The acquisition function, specifically the robust EI, integrates information from the posterior mean and SD to guide the BO process. Brighter regions correspond to high acquisition values, indicating areas that balance high predicted impact velocity with high uncertainty. In particular, *region with a channel angle of approximately 55-65 degrees and a channel diameter of 6-9 mm* shows a strong alignment between AF and the posterior mean, suggesting it as a prime candidate for further exploration. This ensures an effective trade-off between exploration (reducing uncertainty) and exploitation (maximizing impact velocity), ultimately refining the design optimization process.

4.4.2. Validation of the GP Regression Model

To assess the performance of the GP regression model in predicting impact velocity (V), the dataset was split into 90% training data and 10% test data. This split ensures that the model is trained on a sufficient amount of data while reserving an independent test set for evaluating its predictive accuracy. Two standard regression metrics, Mean Absolute Error (MAE) and Root Mean Squared Error (RMSE), were used to quantify the model's performance [24]. These metrics provide complementary insights by measuring both the average magnitude of errors and the variability in prediction accuracy. For the GP model, the computed error metrics are:

$$\text{MAE} = 94.72\ \text{m/s}, \quad \text{RMSE} = 109.44\ \text{m/s}.$$

The MAE and RMSE values indicate relatively large errors, suggesting potential limitations in the GP model's ability to fully capture the complex relationships within the five-dimensional design space. These errors likely stem from the high-dimensionality of the design space and the limited number of evaluation points (276), which may not sufficiently represent the nonlinear behavior across the entire domain.

To further analyze the predictive performance of the model, a scatter plot of predicted vs. actual impact velocities is shown in Figure 5. The 45-angle dashed line (i.e., $y = x$) represents the line of ideal prediction. The proximity of scatter points to this line reflects the model's accuracy, with larger deviations indicating higher prediction errors.

Overall, while the GP model provides reasonable approximations of impact velocity, further improvements may be necessary to enhance predictive accuracy. Potential strategies include increasing the number of training samples, refining hyperparameter tuning, or integrating additional constraints to improve generalization across the design space.

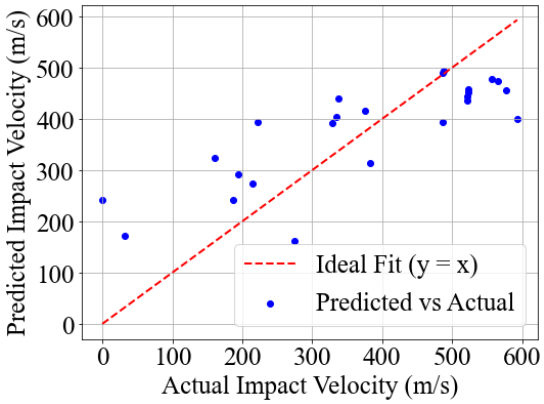

FIGURE 5: SCATTER PLOT OF PREDICTED VS. ACTUAL IMPACT VELOCITIES. THE RED DASHED LINE REPRESENTS THE IDEAL FIT, INDICATING PERFECT PREDICTIONS. THE DATASET WAS SPLIT INTO 90% TRAINING AND 10% TEST DATA.

5. CONCLUSION

The paper presents a constrained Bayesian Optimization (BO) framework tailored for robust design, optimizing both performance and consistency across varying operating conditions. Using condition-specific Gaussian process (GP) submodels, the proposed methodology is capable of capturing the non-linear relationship between design parameters and performance outcomes under diverse conditions. The integration of consistency constraints through a new robust Expected Improvement (EI) criterion effectively guides the search process toward stable, high-performing designs, balancing exploration and exploitation. The approach is demonstrated through a cold-spray nozzle design, which successfully achieves the maximum impact velocity while ensuring stability in multiple operating scenarios. The results confirm the efficacy of the framework in identifying high-quality, robust designs, making it a valuable tool for practical engineering optimization problems.

While this study demonstrates promising results, there are several limitations to consider. For instance, the validation of the GP model still exhibits relatively large errors, primarily due to the complexity and high dimensionality of the design space. In future work, we plan to adopt our previous work on multi-agent Bayesian optimization [25, 26], leveraging multiple parallel GP models to improve predictive accuracy and computational scalability. Additionally, the determination of the trade-off parameter λ between maximizing performance and ensuring robustness across conditions in Eq. (18) is still somewhat subjective. To address this, we aim to investigate signal-to-noise ratio (SNR) metrics [27] acquisition functions that preserve statistical consistency and offer more intuitive control for designers. Lastly, we plan to extend the approach to higher-dimensional design problems, conduct additional case studies across diverse engineering domains, and evaluate the robustness of the optimized designs under broader variations in operating conditions.

ACKNOWLEDGMENTS

The authors gratefully acknowledge the financial support from the National Science Foundation through the grant CMMI-2321463.

REFERENCES

[1] Forrester, Alexander IJ, Sobester, Andras and Keane, Andy J. "Engineering Design via Surrogate Modelling: A Practical Guide." *Wiley* (2008).

[2] Shan, Songqing and Wang, G Gary. "Survey of modeling and optimization strategies to solve high-dimensional design problems with computationally-expensive black-box functions." *Structural and multidisciplinary optimization* Vol. 41 (2010): pp. 219–241.

[3] Frazier, Peter I. "A tutorial on Bayesian optimization." *arXiv preprint arXiv:1807.02811* (2018).

[4] Snoek, Jasper, Larochelle, Hugo and Adams, Ryan P. "Practical bayesian optimization of machine learning algorithms." *Advances in neural information processing systems* Vol. 25 (2012).

[5] Shahriari, Bobak, Swersky, Kevin, Wang, Ziyu, Adams, Ryan P and De Freitas, Nando. "Taking the human out of the loop: A review of Bayesian optimization." *Proceedings of the IEEE* Vol. 104 No. 1 (2015): pp. 148–175.

[6] Bierschenk, Stephen G and Kovar, Desiderio. "Micro-cold Spray Deposition of YSZ Films from Ultrafine Powders Using a Pressure Relief Channel Nozzle." *Journal of Thermal Spray Technology* Vol. 33 No. 6 (2024): pp. 2022–2033.

[7] Mialon, Bruno, Fol, Thierry and Bonnaud, Cyril. "Aerodynamic optimization of subsonic flying wing configurations." *20th AIAA applied aerodynamics conference*: p. 2931. 2002.

[8] Guest, James K and Igusa, Takeru. "Structural optimization under uncertain loads and nodal locations." *Computer Methods in Applied Mechanics and Engineering* Vol. 198 No. 1 (2008): pp. 116–124.

[9] Xia, Quangang, Zhang, Tong, Sun, Zhifei and Gao, Yuan. "Design and optimization of thermal strategy to improve the thermal management of proton exchange membrane fuel cells." *Applied Thermal Engineering* Vol. 222 (2023): p. 119880.

[10] Gardner, Jacob R., Kusner, Matt J., Xu, Zhixiang, Weinberger, Kilian Q. and Cunningham, John P. "Bayesian optimization with inequality constraints." *Proceedings of the 31st International Conference on Machine Learning (ICML-14)*: pp. 937–945. 2014. URL https://proceedings.mlr.press/v32/gardner14.pdf.

[11] Wang, J., Petra, C. G. and Peterson, J. L. "Constrained Bayesian optimization with merit functions." *arXiv preprint arXiv:2403.13140* (2024).

[12] Zhang, Yunxiang, Zhang, Xiangyu and Frazier, Peter. "Constrained two-step look-ahead Bayesian optimization." *Advances in Neural Information Processing Systems*. 2021.

[13] Christianson, Ryan B. and Gramacy, Robert B. "Robust expected improvement for Bayesian optimization." *arXiv preprint arXiv:2302.08612* (2023)URL https://arxiv.org/abs/2302.08612.

[14] Bogunovic, Ilija, Scarlett, Jonathan, Jegelka, Stefanie and Cevher, Volkan. "Adversarially robust optimization with Gaussian processes." *Advances in neural information processing systems* Vol. 31 (2018).

[15] Marzat, Julien, Walter, Eric and Piet-Lahanier, Hélène. "Worst-case global optimization of black-box functions through Kriging and relaxation." *Journal of Global Optimization* Vol. 55 (2013): pp. 707–727.

[16] Srinivas, Niranjan, Krause, Andreas, Kakade, Sham M and Seeger, Matthias. "Gaussian process optimization in the bandit setting: No regret and experimental design." *arXiv preprint arXiv:0912.3995* (2009).

[17] Rasmussen, Carl Edward. "Gaussian processes in machine learning." *Summer school on machine learning*: pp. 63–71. 2003. Springer.

[18] Bierschenk, Stephen G and Kovar, Desiderio. "A nozzle design for mitigating particle slowing in the bow shock region during micro-cold spray of 8 YSZ films." *Journal of Aerosol Science* Vol. 179 (2024): p. 106360.

[19] Assadi, Hamid, Schmidt, T, Richter, H, Kliemann, J-O, Binder, K, Gärtner, F, Klassen, T and Kreye, H. "On parameter selection in cold spraying." *Journal of thermal spray technology* Vol. 20 (2011): pp. 1161–1176.

[20] Yin, Shuo, Meyer, Morten, Li, Wenya, Liao, Hanlin and Lupoi, Rocco. "Gas flow, particle acceleration, and heat transfer in cold spray: a review." *Journal of Thermal Spray Technology* Vol. 25 (2016): pp. 874–896.

[21] Hanft, Dominik, Exner, Jörg, Schubert, Michael, Stöcker, Thomas, Fuierer, Paul and Moos, Ralf. "An overview of the aerosol deposition method: Process fundamentals and new trends in materials applications." *J. Ceram. Sci. Technol* Vol. 6 No. 3 (2015): pp. 147–182.

[22] COMSOL AB. *COMSOL Multiphysics® v. 6.3*. COMSOL AB, Stockholm, Sweden (2024). URL https://www.comsol.com.

[23] Henderson, Charles B. "Drag coefficients of spheres in continuum and rarefied flows." *AIAA journal* Vol. 14 No. 6 (1976): pp. 707–708.

[24] Willmott, Cort J and Matsuura, Kenji. "Advantages of the mean absolute error (MAE) over the root mean square error (RMSE) in assessing average model performance." *Climate research* Vol. 30 No. 1 (2005): pp. 79–82.

[25] Chen, Siyu, Bayrak, Alparslan Emrah and Sha, Zhenghui. "A Cost-Aware Multi-Agent System for Black-Box Design Space Exploration." *Journal of Mechanical Design* Vol. 147 No. 1 (2025): p. 011703.

[26] Chen, Siyu, Bayrak, Alparslan Emrah and Sha, Zhenghui. "Distributed Multi-Agent Bayesian Optimization for Unknown Design Space Exploration." *International Design Engineering Technical Conferences and Computers and Information in Engineering Conference*, Vol. 88377: p. V03BT03A040. 2024. American Society of Mechanical Engineers.

[27] Taguchi, Genichi. "Robust technology development." *Mechanical Engineering-CIME* Vol. 115 No. 3 (1993): pp. 60–63.